

# Non-Fermi-liquid behavior in cubic phase BaRuO<sub>3</sub>: A dynamical mean-field study

Li Huang<sup>1,2</sup> and Bingyun Ao<sup>2</sup>

<sup>1</sup>*Beijing National Laboratory for Condensed Matter Physics,  
and Institute of Physics, Chinese Academy of Sciences, Beijing 100190, China*

<sup>2</sup>*Science and Technology on Surface Physics and Chemistry Laboratory,  
P.O. Box 718-35, Mianyang 621907, Sichuan, China*

(Dated: March 8, 2013)

## Abstract

Motivated by the recently synthesized cubic phase BaRuO<sub>3</sub> under high pressure and high temperature, a thorough study has been conducted on its temperature-dependent electronic properties by using the state-of-the-art *ab initio* computing framework of density functional theory combined with dynamical mean-field theory. At ambient condition the cubic phase BaRuO<sub>3</sub> should be a weakly correlated Hund's metal with local magnetic moment. The spin-spin correlation function and local magnetic susceptibility can be well described by the Curie-Weiss law over a wide temperature range. The calculated low-frequency self-energy functions of Ru-4d states apparently deviate from the behaviors predicted by Landau Fermi-liquid theory. Beyond that, the low-frequency optical conductivity can be fitted to a power-law  $\Re\sigma(\omega) \sim \omega^{-0.98}$ , which further confirms the Non-Fermi-liquid metallic state.

PACS numbers: 71.30.+h, 71.27.+a, 75.30.Wx

## I. INTRODUCTION

Recently the alkaline-earth ruthenium oxides have attracted growing interest. These oxides generally exhibit fascinating physics properties, such as unconventional superconductivity with  $p$ -wave symmetry ( $\text{Sr}_2\text{RuO}_4$ ),<sup>1</sup> antiferromagnetic Mott insulator ( $\text{Ca}_2\text{RuO}_4$ ),<sup>2</sup> and orbital selective Mott transition in  $\text{Sr}_{2-x}\text{Ca}_x\text{RuO}_4$ ,<sup>3</sup> etc. Among the rest, due to their interesting magnetic phase diagrams, transport properties and potential device applications, the ternary ruthenates with perovskite or perovskite-related structures ( $\text{ARuO}_3$ :  $\text{A} = \text{Ca}, \text{Sr}, \text{Ba}$ ) have been extensively studied by numerous experiments and theoretical calculations in the past decade.<sup>4-17</sup>

Both  $\text{CaRuO}_3$  and  $\text{SrRuO}_3$  crystallize in the orthorhombic perovskite structure with a  $\text{GdFeO}_3$ -type distortion.  $\text{SrRuO}_3$  is a highly correlated, narrow-band metallic ferromagnet with a Curie temperature ( $T_c$ ) of about 160 K.<sup>4</sup> Its local magnetic moment ( $1.4 \mu_B$ ) is rather large, despite highly extended  $4d$  character of the valence electrons. Interestingly,  $\text{CaRuO}_3$ , an isostructural compound, does not show any magnetic ordering in finite temperatures.<sup>5</sup> The nature of its magnetic ground state still remains controversial. We note that one of the most striking properties of  $\text{CaRuO}_3$  and  $\text{SrRuO}_3$  compounds is the violation of Landau Fermi-liquid (LFL) theory, which has been proven by many experimental results, including x-ray photoemission spectra, transport and optical properties, etc.<sup>6-9</sup> The strength of Coulomb interaction  $U$  and the importance of Hund's rule coupling  $J$  among Ru- $4d$  orbitals are another two interesting topics and in lively debate. Though almost all the experimental<sup>10-12</sup> and theoretical<sup>13-15</sup> efforts manifest some role of electron-electron correlation, the strength and the extent of its importance still remain unclear.

In the earlier years, it is well known that depending on how  $\text{BaRuO}_3$  is synthesized it has several polytype structures, i.e., the nine-layered rhombohedral (9R), the four layered hexagonal (4H), and the six layered hexagonal (6H).<sup>16,17</sup> Lately, the cubic phase  $\text{BaRuO}_3$  with ideal perovskite structure has been synthesized by Jin *et al.* under 18 GPa at 1000 °C.<sup>18</sup> It remains metallic down to 4 K and occurs a ferromagnetic transition at  $T_c = 60$  K,<sup>19</sup> which is significantly lower than that of  $\text{SrRuO}_3$ .<sup>4</sup> The ferromagnetic transition in  $\text{SrRuO}_3$  falls into the mean-field universality class whereas cubic phase  $\text{BaRuO}_3$  exhibits significant critical fluctuations as described by the 3D Heisenberg model.<sup>19</sup> The availability of cubic phase  $\text{BaRuO}_3$  not only completes the polymorph of  $\text{BaRuO}_3$ , but also makes it possible to

map out the evolution of magnetism and other properties as a function of the ionic size of the A-size in the whole series of  $\text{ARuO}_3$ .<sup>18</sup>

Despite tremendous efforts have been made, little is known about the basic properties of cubic phase  $\text{BaRuO}_3$ . In this paper, we will address the following two issues: (i) Definitely, in  $\text{CaRuO}_3$  and  $\text{SrRuO}_3$ , the effects induced by electronic correlation can not be ignored.<sup>10–15</sup> However, does the electronic correlation play a decisive role in cubic phase  $\text{BaRuO}_3$ ? (ii) It is believed that the physical properties of  $\text{CaRuO}_3$  and  $\text{SrRuO}_3$  can not be well described by the LFL theory. Indeed, the evidences are their low-frequency optic conductivity, resistivity, and electronic Raman scattering intensity which obey the fractional power-law.<sup>6–9</sup> Thus, whether the physical properties of cubic phase  $\text{BaRuO}_3$  still violate the LFL theory is an essential problem.

The density functional theory within local density approximation combined with dynamical mean-field theory (dubbed LDA + DMFT) is a very powerful computing framework for strongly correlated materials.<sup>20–22</sup> In the present works, by employing the LDA + DMFT computational scheme, the temperature-dependent electronic properties of cubic phase  $\text{BaRuO}_3$  have been systematically studied. In contrast to  $\text{CaRuO}_3$  and  $\text{SrRuO}_3$ , under room temperature cubic phase  $\text{BaRuO}_3$  is a weakly correlated Hund’s metal with local magnetic moment, and its low-frequency conductivity deviates the  $\omega^{-2}$  law as is predicted by classic LFL theory.

## II. METHOD

We first compute the ground state electronic structures of cubic phase  $\text{BaRuO}_3$  within nonmagnetic configuration by utilizing the plane-wave pseudopotential approach as is implemented in the QUANTUM ESPRESSO software package.<sup>23</sup> The generalized gradient approximation with Perdew-Burke-Ernzerhof exchange-correlation functional<sup>24</sup> is used to describe the exchange and correlation potentials. The pseudopotentials in projector augmented wave scheme<sup>25</sup> for Ba, Ru, and O species are built by ourselves. The electronic wave functions are described with a plane-wave basis truncated at 80 Ha, and a  $\Gamma$ -centered  $12 \times 12 \times 12$   $k$ -point grid for Brillouin zone integrations is adopted. These pseudopotentials and computational parameters are carefully checked and tuned to ensure the numerical convergences.

To include the effect of electronic correlation, the ground state wave functions are used

to construct a basis of maximally localized Wannier functions (MLWF) for Ru-4*d* and O-2*p* orbitals. The corresponding multiband Hubbard Hamiltonian has the following form<sup>21,22</sup>

$$H_{\text{LDA+DMFT}} = H_{\text{LDA}} - H_{\text{DC}} + \sum_{imm'} \frac{U_{mm'}}{2} n_{im} n_{im'}, \quad (1)$$

where  $n_{im} = c_{im}^\dagger c_{im}$ , and  $c_{im}^\dagger (c_{im})$  creates (destroys) an electron in a Wannier orbital  $m$  at site  $i$ . Here  $H_{\text{LDA}}$  is the effective low-energy Hamiltonian in the basis of Ru-4*d* and O-2*p* MLWF orbitals, and thus is a  $14 \times 14$  matrix.  $H_{\text{DC}}$  is a double counting correction term which accounts for the electronic correlation already described by the LDA part, and the fully local limit scheme<sup>26</sup> is chosen. The Coulomb interaction is taken into considerations merely among the Ru-4*d* orbitals. We use  $U = 4.0$  eV and  $J = 0.65$  eV to parameterize the Coulomb interaction matrix, which are close to previous estimations.<sup>14,15</sup> To solve the many-body Hamiltonian (1), in the DMFT part<sup>20,21</sup> we employ the hybridization expansion continuous time quantum Monte Carlo impurity solver (abbreviated CT-HYB).<sup>27,28</sup> Finally, through the mature analytical continuation methods<sup>29,30</sup> the impurity spectral function can be extracted directly from the imaginary-time Green's function which are derived from the quantum Monte Carlo simulations.

### III. RESULTS AND DISCUSSION

Figure 1 represents our calculated orbital-resolved density of states for Ru-4*d* states at several typical temperatures. The octahedral surrounding of Ru splits the Ru-4*d* states into three-fold degenerated  $t_{2g}$  and two-fold degenerated  $e_g$  levels. Ru<sup>4+</sup> ion, which is nominally in a low-spin,  $d^4$  configuration, gives rise to a  $t_{2g}^4$  configuration with Fermi level lying in the  $t_{2g}$  manifold with empty  $e_g$  states. As for the density of states of  $t_{2g}$  states, it displays a sharp quasiparticle peak near the Fermi level, a shoulder structure around -0.3 eV, and a Hubbard subband like hump at -8.0 eV  $\sim$  -2.0 eV. While for the density of states of  $e_g$  states, since it is less occupied, the primary spectral weight is above the Fermi level. There are two small satellites located on both sides of the Fermi level (-0.1 and 0.3 eV, respectively). With the increment of temperature, the two peaks will be smeared out gradually. To sum up, the integrated spectral functions of Ru-4*d* states show significantly metallic features, and the temperature effect is not very obvious. When the temperature rises from 190 K to 580 K, slightly spectral weight transfer to high energy is observed.

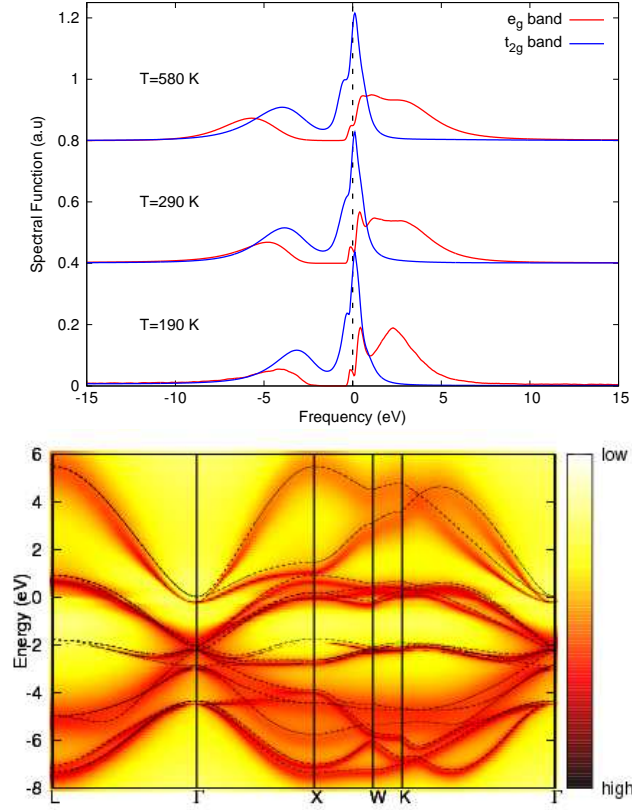


FIG. 1. (Color online) Spectral functions of cubic perovskite BaRuO<sub>3</sub> calculated by LDA + DMFT method. Upper panel: Spectral functions of Ru-4d states at various temperatures. Lower panel: Quasiparticle band structure of BaRuO<sub>3</sub> along high symmetry lines in the Brillouin zone.

In the next step, we computed the full momentum-resolved spectral function  $A(k, \omega)$  along some high symmetry lines in the Brillouin zone for cubic phase BaRuO<sub>3</sub>. The inverse temperature  $\beta$  is chosen to be 40, which corresponding to  $T = 290$  K approximately. In the lower panel of Fig.1  $A(k, \omega)$  is shown in comparison with the LDA band structure. The sharp quasiparticle peak observed in the integrated spectral function is clearly visible on the intensity plot, and fairly well defined. It lies in the region about from -2.0 eV to 1.5 eV, dominated by the  $t_{2g}$  states. At higher energy, the  $e_g$  states become the majority. However, in the region below -2.0 eV, the O-2p states make a major contribution. From the distribution of spectral weights of  $t_{2g}$  and  $e_g$  states, it is speculated that in the region from -2.0 eV to -7.0 eV, there exists strong hybridization between the Ru-4d and O-2p states. Comparing this with the LDA band structure, first of all we notice the quasiparticle band structure does not show apparent shifting. Secondly, except for becoming diffuse,

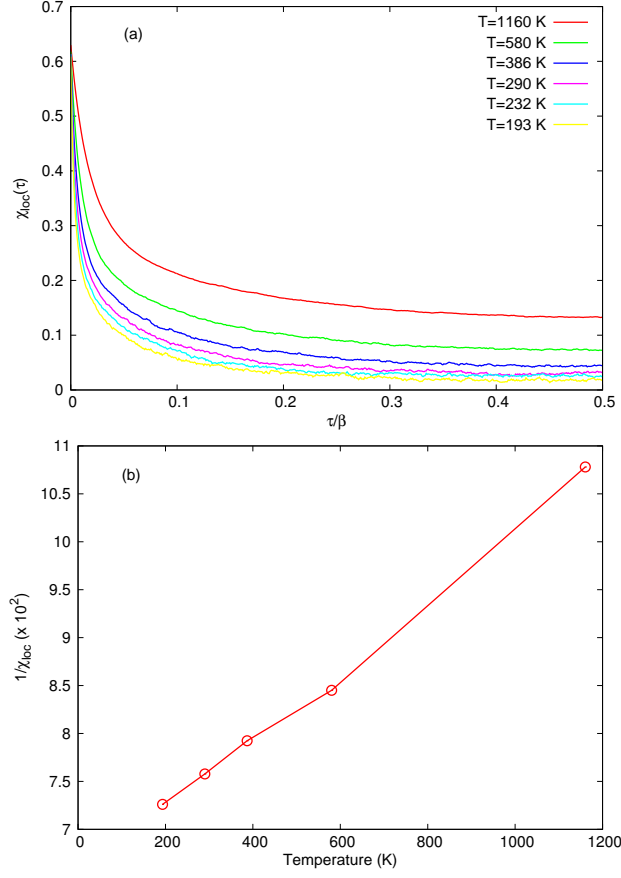


FIG. 2. (Color online) Magnetic properties of cubic perovskite BaRuO<sub>3</sub>. (a) Spin-spin correlation functions  $\chi(\tau) = \langle S_z(0)S_z(\tau) \rangle$  at various temperatures. (b) Inverse local magnetic susceptibility  $\chi_{loc}^{-1}$  as a function of temperature.

the band renormalization of the quasiparticle band structure is hard to be distinguished. In general, the quasiparticle band structure of cubic phase BaRuO<sub>3</sub> coincides with its LDA band structure, giving rise to a picture of weakly correlated metal. On the contrary, previous LDA + DMFT calculations for CaRuO<sub>3</sub> and SrRuO<sub>3</sub> present strongly renormalized and shifted quasiparticle band structure,<sup>14</sup> resulting in the picture of moderately correlated metal.

In recent years, the evolutional trend of ferromagnetism in ARuO<sub>3</sub> is in hot debate.<sup>5,18,19</sup> Thus in the present works, we calculated the spin-spin correlation function  $\chi(\tau)$  and local magnetic susceptibility  $\chi_{loc}$  of cubic phase BaRuO<sub>3</sub>, and tried to elucidate its magnetic properties in finite temperatures. The calculated spin-spin correlation functions are illustrated in Fig.2(a). On one hand, the cubic phase BaRuO<sub>3</sub> exhibits a well-defined frozen local moment, which is characterized by a spin-spin correlation function that approaches non-zero

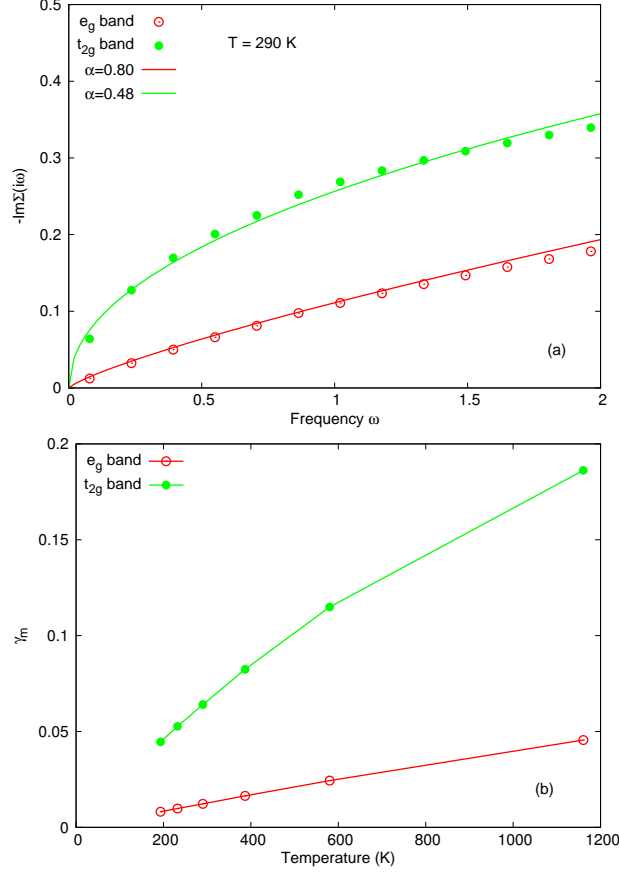


FIG. 3. (Color online) Electronic self-energy function of Ru-4d states. (a) Imaginary part of the Matsubara self-energy function  $\Im\Sigma(i\omega)$  for  $t_{2g}$  and  $e_g$  orbitals at  $T = 290$  K. The solid lines denote as the fitted function  $-\Im\Sigma(i\omega) = A(i\omega)^\alpha + B$ . (b) Orbital-resolved low-energy scattering rate  $\gamma_m = -\Im\Sigma_m(i\omega \rightarrow 0)$ .

constants at large enough  $\tau$ , as is easily seen from  $T = 193$  K to 1160 K. On the other hand, the spin-spin correlation function does not behave as  $\chi(\tau) \sim (T/\sin(T\tau\pi))^2$  for times  $\tau$  sufficiently far from  $\tau = 0$  or  $\beta$  respectively, which means the violation of LFL theory.<sup>31</sup> From the spin-spin correlation function, the local magnetic susceptibility  $\chi_{loc} = \int_0^\beta \chi(\tau) d\tau$  can be easily evaluated, which is plotted in Fig.2(b). As shown, the calculated  $\chi_{loc}$  is Curie-Weiss like over a rather wide temperature range, in other words, it follows a  $\chi_{loc}^{-1}(T) = T/C$  law at least up to  $T = 1160$  K. This implies that the Ru-4d electrons in cubic phase BaRuO<sub>3</sub> retain the local nature of the magnetic moment.

Next we concentrate our attentions to the electronic self-energy functions of Ru-4d states. The calculated orbital-resolved  $\Im\Sigma(i\omega)$  are shown in Fig.3(a). For the sake of simplicity,

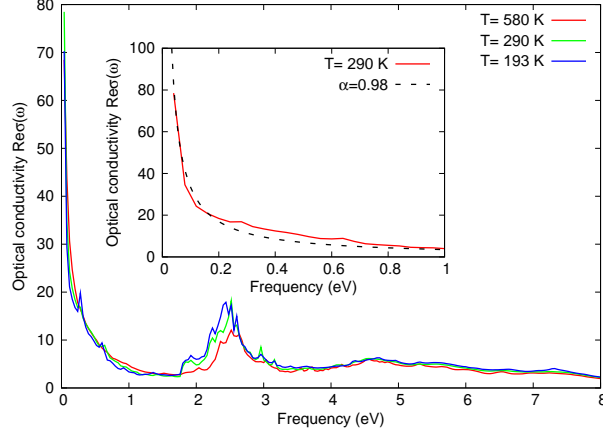


FIG. 4. (Color online) Real part of optical conductivity of cubic perovskite BaRuO<sub>3</sub> by LDA + DMFT calculations. Inset: The low-frequency  $\Re\sigma(\omega)$  at  $T = 290$  K, and the dashed line represents the fitted function  $\Re\sigma(\omega) = C\omega^{-\alpha}$ .

only those results calculated at  $T = 290$  K are presented. Werner *et al.*<sup>31</sup> have suggested that the still-mysterious optical conductivity  $\sigma(\omega)$  in pseudocubic SrRuO<sub>3</sub> and CaRuO<sub>3</sub>, which varies approximately as  $\omega^{-0.5}$  and deviates sharply from the prediction of LFL theory, can be perfectly interpreted as a consequence of square-root self-energy function. Inspired by their works, we conducted a careful analysis to determine the asymptotically formula for the low-frequency self-energy function. In a Fermi-liquid, the imaginary part of Matsubara self-energy should exhibit a linear regime at low energy, whose slope is directly related to the quasiparticle mass enhancement. However, as shown in Fig.3(a), we do not observe any linear behavior: the Matsubara self-energy behaves as  $-\Im\Sigma(i\omega) = A(i\omega)^\alpha + \gamma$  with  $\alpha \sim 0.48$  for  $t_{2g}$  states and  $\alpha \sim 0.80$  for  $e_g$  states, respectively. The non-linear frequency dependence of the Matsubara self-energy implies that Landau quasiparticles and effective masses can not be properly defined for cubic phase BaRuO<sub>3</sub>. The non-zero intercept  $\gamma = -\Im\Sigma(i\omega \rightarrow 0)$  can be viewed as the low-energy scattering rate and it is a broadly used physical quantity to distinguish the LFL and NFL phases.<sup>31</sup> As a byproduct, the orbital-resolved  $\gamma_m$  is evaluated as a function of temperature and shown in Fig.3(b). Clearly,  $\gamma_m$  increases monotonously with the increment of temperature and  $\gamma_{t_{2g}} > \gamma_{e_g}$  is always valid. For both  $t_{2g}$  and  $e_g$  states  $\gamma_m$  can not be neglected even at  $T = 190$  K. Thus, it means that similar to SrRuO<sub>3</sub> and CaRuO<sub>3</sub>, the cubic phase BaRuO<sub>3</sub> lies in the NFL regime as well.

A power-law analysis on the transport properties, such as resistivity  $\rho(T) \propto T^n$ , of cubic



phase BaRuO<sub>3</sub> was made by Zhou *et al.*<sup>19</sup> and the exponent  $n$  as a function of pressure was evaluated recently. Their results show an interesting evolution from  $n \sim 1.85$ , which is close to  $n = 2$  for the LFL phase at ambient pressure, to  $n \sim 1.4$  of the NFL phase at the pressure where the ferromagnetic phase collapses. The most important evidence for NFL state in SrRuO<sub>3</sub> and CaRuO<sub>3</sub> is the fractional power-law conductivity.<sup>6-8</sup> In this work, we also calculate the optical conductivity  $\sigma(\omega)$  of cubic phase BaRuO<sub>3</sub> under various temperatures. In Fig.4 only the real part of optical conductivity is shown. The sharp peak near  $\omega = 0$  denotes the Drude-like feature. The broad hump located from 1.5 eV to 3.5 eV can be attributed to the contribution of electron transition between quasiparticle peak and Hubbard subbands.<sup>11</sup> With the increment of temperature, this hump slightly shifts to higher frequency region, which is in accord with the variation trend of Hubbard subbands observed in the temperature-dependent integrated spectral functions of Ru-4d states (see Fig.1). In order to further confirm whether the underlying physics of cubic phase BaRuO<sub>3</sub> can be described with LFL theory, we conduct a detailed power-law analysis for the low-frequency optical conductivity at  $T = 290$  K. The low-frequency optical conductivity is fitted by the exponent function  $\Re\sigma(\omega) \sim C\omega^{-\alpha}$ . The quantitative results are shown in the inset of Fig.4. The fitted exponent  $\alpha \sim 0.98$ , while the expected value predicted by LFL theory is  $\alpha = 2$ . It's worth mentioning that the exponent  $\alpha$  is approximately 0.5 for pseudocubic SrRuO<sub>3</sub> and CaRuO<sub>3</sub>, and 0.7 for some high temperature superconductivity cuprates.<sup>6,7</sup> Nevertheless, the optical conductivity data suggest the NFL metallic nature of cubic phase BaRuO<sub>3</sub> under ambient condition again.

Finally, we should emphasize the importance of Hund's physics in cubic phase BaRuO<sub>3</sub>. Very recent investigations about iron pnictides and chalcogenides showed that strong correlation is not always caused by the Hubbard interaction  $U$ , but can arise from the Hund's rule coupling  $J$ .<sup>32,33</sup> Since the strength of electronic correlation in these materials is almost entirely due to the Hund's rule coupling, they are dubbed Hund's metals by Haule *et al.*<sup>32</sup> at first. It has recently been noticed by Yin *et al.* that in realistic Hund's metals, the electronic self-energy and corresponding optical conductivity show NFL power-law frequency dependence, tendency towards strong orbital differentiation, and that large mass enhancement can occur even though no clear Hubbard subband exist in the single particle spectra.<sup>31,33-35</sup> According to their investigations, both the iron pnictides and chalcogenides are typical Hund's metals. The origin of fractional power-law in the optical conductivity of

them can be traced to the Hund's rule interaction. As for the cubic phase BaRuO<sub>3</sub>, based on our calculated results: NFL behavior in low-frequency self-energy function and scattering rate, fractional power-law in the optical conductivity, and considerable mass enhancement (at  $T = 290$  K  $m_{t_{2g}}^* = 1.8m_0$  and  $m_{e_g}^* = 1.2m_0$ ), we can conclude that it is another realistic Hund's metal. Indeed, we have performed additional LDA + DMFT calculations for cubic phase BaRuO<sub>3</sub> with different Coulomb interaction strengths from  $U = 2.0$  eV to  $6.0$  eV and obtained almost identical results. However, when  $U = 4.0$  eV and the Hund's rule coupling term is completely ignored ( $J = 0.0$  eV), the NFL behaviors previously found in the self-energy function and optical conductivity are absent totally. It should be noted that Medici *et al.*<sup>36</sup> have suggested that the physical properties of ruthenates are governed by the Hund's physics, in other words, the perovskite ARuO<sub>3</sub> forms a new series of Hund's metal. Our calculated results for the cubic phase BaRuO<sub>3</sub> confirm their issue as well.

#### IV. SUMMARY

In summary, to find out a consistent description for the ARuO<sub>3</sub>-type ruthenates, we study the temperature-dependent physical properties of recently synthesized cubic phase BaRuO<sub>3</sub> by using the first principles LDA + DMFT approach. Judged from the quasiparticle band structure and integrated spectral functions of Ru-4*d* states, the cubic phase BaRuO<sub>3</sub> is a weakly correlated Hund's metal. There exists local magnetic moment and the inverse local magnetic susceptibility obeys the Curie-Weiss law in the studied temperature regime. The low-frequency self-energy function, scattering rate, and optical conductivity of cubic phase BaRuO<sub>3</sub> show apparent NFL behaviors. It is argued that the Hund's rule coupling  $J$  plays an important role in the underlying physics in cubic phase BaRuO<sub>3</sub> and other perovskite ARuO<sub>3</sub> compounds.

#### ACKNOWLEDGMENTS

LH was supported by the National Science Foundation of China and that from the 973 program of China under Contract No.2007CB925000 and No.2011CBA00108. BYA was

supported by the National Science Foundation of China under Contract No.20971114.

---

- <sup>1</sup> Y. Maeno, H. Hashimoto, K. Yoshida, S. Nishizaki, T. Fujita, J. G. Bednorz, and F. Lichtenberg, *Nature* **372**, 532 (1994).
- <sup>2</sup> S. Nakatsuji and Y. Maeno, *Phys. Rev. Lett.* **84**, 2666 (2000).
- <sup>3</sup> V. I. Anisimov, I. A. Nekrasov, D. E. Kondakov, T. M. Rice, and M. Sigrist, *Eur. Phys. J. B* **25**, 191 (2002).
- <sup>4</sup> G. Koster, L. Klein, W. Siemons, G. Rijnders, J. S. Dodge, C.-B. Eom, D. H. A. Blank, and M. R. Beasley, *Rev. Mod. Phys.* **84**, 253 (2012).
- <sup>5</sup> G. Cao, S. McCall, M. Shepard, J. E. Crow, and R. P. Guertin, *Phys. Rev. B* **56**, 321 (1997).
- <sup>6</sup> P. Kostic, Y. Okada, N. C. Collins, Z. Schlesinger, J. W. Reiner, L. Klein, A. Kapitulnik, T. H. Geballe, and M. R. Beasley, *Phys. Rev. Lett.* **81**, 2498 (1998).
- <sup>7</sup> J. S. Dodge, C. P. Weber, J. Corson, J. Orenstein, Z. Schlesinger, J. W. Reiner, and M. R. Beasley, *Phys. Rev. Lett.* **85**, 4932 (2000).
- <sup>8</sup> Y. S. Lee, J. Yu, J. S. Lee, T. W. Noh, T.-H. Gimm, H.-Y. Choi, and C. B. Eom, *Phys. Rev. B* **66**, 041104 (2002).
- <sup>9</sup> M. S. Laad, I. Bradarić, and F. V. Kusmartsev, *Phys. Rev. Lett.* **100**, 096402 (2008).
- <sup>10</sup> M. Takizawa, D. Toyota, H. Wadati, A. Chikamatsu, H. Kumigashira, A. Fujimori, M. Oshima, Z. Fang, M. Lippmaa, M. Kawasaki, and H. Koinuma, *Phys. Rev. B* **72**, 060404 (2005).
- <sup>11</sup> J. S. Ahn, J. Bak, H. S. Choi, T. W. Noh, J. E. Han, Y. Bang, J. H. Cho, and Q. X. Jia, *Phys. Rev. Lett.* **82**, 5321 (1999).
- <sup>12</sup> K. Maiti and R. S. Singh, *Phys. Rev. B* **71**, 161102 (2005).
- <sup>13</sup> K. Maiti, *Phys. Rev. B* **73**, 235110 (2006).
- <sup>14</sup> E. Jakobi, S. Kanungo, S. Sarkar, S. Schmitt, and T. Saha-Dasgupta, *Phys. Rev. B* **83**, 041103 (2011).
- <sup>15</sup> H. Hadipour and M. Akhavan, *Eur. Phys. J. B* **84**, 203 (2011).
- <sup>16</sup> Y. S. Lee, T. W. Noh, J. H. Park, K.-B. Lee, G. Cao, J. E. Crow, M. K. Lee, C. B. Eom, E. J. Oh, and I.-S. Yang, *Phys. Rev. B* **65**, 235113 (2002).
- <sup>17</sup> C. Felser and R. J. Cava, *Phys. Rev. B* **61**, 10005 (2000).

- <sup>18</sup> C.-Q. Jin, J.-S. Zhou, J. B. Goodenough, Q. Q. Liu, J. G. Zhao, L. X. Yang, Y. Yu, R. C. Yu, T. Katsura, A. Shatskiy, and E. Ito, *Proc. Nat. Acad. Sci.* **105**, 7115 (2008).
- <sup>19</sup> J.-S. Zhou, K. Matsubayashi, Y. Uwatoko, C.-Q. Jin, J.-G. Cheng, J. B. Goodenough, Q. Q. Liu, T. Katsura, A. Shatskiy, and E. Ito, *Phys. Rev. Lett.* **101**, 077206 (2008).
- <sup>20</sup> A. Georges, G. Kotliar, W. Krauth, and M. J. Rozenberg, *Rev. Mod. Phys.* **68**, 13 (1996).
- <sup>21</sup> G. Kotliar, S. Y. Savrasov, K. Haule, V. S. Oudovenko, O. Parcollet, and C. A. Marianetti, *Rev. Mod. Phys.* **78**, 865 (2006).
- <sup>22</sup> B. Amadon, F. Lechermann, A. Georges, F. Jollet, T. O. Wehling, and A. I. Lichtenstein, *Phys. Rev. B* **77**, 205112 (2008).
- <sup>23</sup> P. Giannozzi, S. Baroni, N. Bonini, M. Calandra, R. Car, C. Cavazzoni, D. Ceresoli, G. L. Chiarotti, M. Cococcioni, I. Dabo, A. Dal Corso, S. de Gironcoli, S. Fabris, G. Fratesi, R. Gebauer, U. Gerstmann, C. Gougoussis, A. Kokalj, M. Lazzeri, L. Martin-Samos, N. Marzari, F. Mauri, R. Mazzarello, S. Paolini, A. Pasquarello, L. Paulatto, C. Sbraccia, S. Scandolo, G. Schlauser, A. P. Seitsonen, A. Smogunov, P. Umari, and R. M. Wentzcovitch, *J. Phys: Condens. Matter* **21**, 395502 (2009).
- <sup>24</sup> J. P. Perdew, K. Burke, and M. Ernzerhof, *Phys. Rev. Lett.* **77**, 3865 (1996).
- <sup>25</sup> P. E. Blöchl, *Phys. Rev. B* **50**, 17953 (1994).
- <sup>26</sup> B. Amadon, F. Jollet, and M. Torrent, *Phys. Rev. B* **77**, 155104 (2008).
- <sup>27</sup> P. Werner, A. Comanac, L. de' Medici, M. Troyer, and A. J. Millis, *Phys. Rev. Lett.* **97**, 076405 (2006).
- <sup>28</sup> E. Gull, A. J. Millis, A. I. Lichtenstein, A. N. Rubtsov, M. Troyer, and P. Werner, *Rev. Mod. Phys.* **83**, 349 (2011).
- <sup>29</sup> M. Jarrell and J. Gubernatis, *Phys. Rep.* **269**, 133 (1996).
- <sup>30</sup> K. S. D. Beach, (2004), arXiv:0403055 [cond-mat].
- <sup>31</sup> P. Werner, E. Gull, M. Troyer, and A. J. Millis, *Phys. Rev. Lett.* **101**, 166405 (2008).
- <sup>32</sup> K. Haule and G. Kotliar, *New J. Phys.* **11**, 025021 (2009).
- <sup>33</sup> Z. P. Yin, K. Haule, and G. Kotliar, *Nat. Mater.* **10**, 932 (2011).
- <sup>34</sup> Z. P. Yin, K. Haule, and G. Kotliar, (2012), arXiv:12060801 [cond-mat].
- <sup>35</sup> A. Kutepov, K. Haule, S. Y. Savrasov, and G. Kotliar, *Phys. Rev. B* **82**, 045105 (2010).
- <sup>36</sup> L. de' Medici, J. Mravlje, and A. Georges, *Phys. Rev. Lett.* **107**, 256401 (2011).